Journal of Solid State Chemistry 183 (2010) 940–950

Contents lists available at ScienceDirect

Journal of Solid State Chemistry

journal homepage: www.elsevier.com/locate/jssc

Crystal structure, microstructure and reducibility of $LaNi_xCo_{1-x}O_3$ and $LaFe_xCo_{1-x}O_3$ Perovskites ($0 < x \leq 0.5$)

S. Ivanova [a], A. Senyshyn [b], E. Zhecheva [a], K. Tenchev [c], R. Stoyanova [a,*], H. Fuess [b]

[a] Institute of General and Inorganic Chemistry, Bulgarian Academy of Sciences, Sofia 1113, Bulgaria
[b] Darmstadt University of Technology, Institute of Materials Science, Structure Research, Petersenstr. 23, D-64287, Germany
[c] Institute of Catalysis, Bulgarian Academy of Sciences, Sofia 1113, Bulgaria

ARTICLE INFO

Article history:
Received 1 July 2009
Received in revised form
3 February 2010
Accepted 11 February 2010
Available online 18 February 2010

Keywords:
Cobalt perovskites
Synthesis
Reduction
X-ray diffraction
Neutron diffraction
Electron paramagnetic resonance

ABSTRACT

Nickel and iron substituted $LaCoO_3$ with rhombohedrally distorted perovskite structure were obtained in the temperature range of 600–900 °C by thermal decomposition of freeze-dried citrates and by the Pechini method. The crystal structure, morphology and defective structure of $LaCo_{1-x}Ni_xO_3$ and $LaCo_{1-x}Fe_xO_3$ were characterized by X-ray diffraction and neutron powder diffraction, TEM and SEM analyses and electron paramagnetic resonance spectroscopy. The reducibility was tested by temperature programmed reduction with hydrogen. The products of the partial and complete reduction were determined by *ex-situ* XRD experiments. The replacement of Co by Ni and Fe led to lattice expansion of the perovskite structure. For perovskites annealed at 900 °C, there was a random Ni, Fe and Co distribution. The morphology of the perovskites does not depend on the Ni and Fe content, nor does it depend on the type of the precursor used. $LaCo_{1-x}Ni_xO_3$ perovskites ($x > 0.1$) annealed at 900 °C are reduced to Co/Ni transition metal and La_2O_3 via the formation of oxygen deficient Brownmillerite-type compositions. For $LaCo_{1-x}Ni_xO_3$ annealed at 600 °C, Co/Ni metal, in addition to oxygen-deficient perovskites, was formed as an intermediate product at the initial stage of the reduction. The interaction of $LaCo_{1-x}Fe_xO_3$ with H_2 occurs by reduction of Co^{3+} to Co^{2+} prior to the Fe^{3+} ions. The reducibility of Fe-substituted perovskites is less sensitive towards the synthesis procedure in comparison with that of Ni substituted perovskites.

1. Introduction

Nickel and iron substituted lanthanum cobaltates with perovskite type structure ($LaCo_{1-x}Ni_xO_3$ and $LaCo_{1-x}Fe_xO_3$) are considered as promising cathode materials for intermediate-temperature solid oxide fuel cells, as well as automotive exhaust catalysts [1–4]. One of the factors determining their cathode and catalytic performance is the mobility of lattice oxygen [5–7]. To evaluate this factor, temperature programmed reduction with H_2 is often used as a fast screening method [5,6]. The reduction of perovskites is a complex process involving the formation of intermediate oxygen-deficient perovskites before the final reduction to metal and La_2O_3. Irrespective of the intensive studies devoted to the reducibility of $LaCo_{1-x}Ni_xO_3$ and $LaCo_{1-x}Fe_xO_3$, the appearance of intermediate phases at the initial stages of reduction is subject to controversial discussions. This is a consequence of the different structural stabilities of oxygen-deficient perovskites [8]. There are two stable oxygen-deficient phases: perovskites from Brownmillerite series ($La_nM_nO_{3n-1}$) and Ruddlesden-Popper phases $La_{m+1}M_mO_{3m+1}$. In the oxygen-deficient phases, Fe ions preferentially occupy octahedral and tetrahedral positions, while Ni ions are in octahedral and square planar positions. This determines the different thermal stability of oxygen-deficient phases. In addition, the stability of these phases depends not only on the nature of transition metal ions, but also on the method of synthesis. Among several synthesis procedures including solution-based and solid state reactions, the most widely used method is the Pechini one [9]. This method is based on the mixing of La and transition metal ions at an atomic scale by the use of citric acid as a chelating agent and of ethylene glycol to form a polyester-type resin [10–12]. Recently, we have demonstrated that the synthesis procedure affects both microstructure and reducibility of unsubstituted $LaCoO_3$ [13]. The different reducibility of $LaCoO_3$ obtained by the Pechini method and that obtained from freeze-dried citrates has been discussed taking into account the formation of oxygen-deficient phases from the Brownmillerite and Ruddlesden-Popper series during the reduction [13]. Here we extend these studies to Ni and Fe substituted $LaCoO_3$ perovskites.

The aim of the present study is to examine the relation between crystal structure, microstructure and reducibility of Ni- and Fe-substituted $LaCoO_3$. Two solution-based methods were

* Corresponding author. Fax: +359 2 870 50 24.
E-mail address: radstoy@svr.igic.bas.bg (R. Stoyanova).

0022-4596/$ - see front matter © 2010 Elsevier Inc. All rights reserved.
doi:10.1016/j.jssc.2010.02.009

used for the preparation of $LaCo_{1-x}Ni_xO_3$ and $LaCo_{1-x}Fe_xO_3$, $0<x\leq 0.5$: the Pechini method and the freeze-dried citrate precursor method. To study the effect of the organic component on the morphology of $LaCoO_3$, the same metal-to-citric acid ratio (La:Co:citric acid=1:1:10) was used with both methods. The thermal properties of freeze-dried citrates and Pechini-type precursors were followed by DTA and TG analysis. Structural and morphological characterization was made by XRD and neutron powder diffraction, TEM and SEM analysis, and specific surface area measurements. Electron paramagnetic resonance spectroscopy (EPR) was used to probe the defect structure of $LaCo_{1-x}Ni_xO_3$ and $LaCo_{1-x}Fe_xO_3$. The reducibility was tested by thermal programmed reduction with hydrogen (TPR). The products of the partial and complete reduction were determined by *ex-situ* XRD experiments.

2. Experimental

Homogeneous La–Co–Ni and La–Co–Fe citrate precursors were obtained by freeze-drying and by a Pechini-type reaction. Lanthanum–cobalt–nickel (or iron) citrates were prepared by adding a 5 M aqueous solution of citric acid (CA) to a suspension of $CoCO_3$, $NiCO_3$ (or $Fe(NO_3)_3$) in aqueous solution of $La(NO_3)_3\cdot 6H_2O$ (1 M La). The ratio between the components was $La:Co_{1-x}M_x:CA=1:1:10$. After stirring, a clear solution was obtained, which was diluted to 0.25 M La ($Co_{1-x}M_x$). For the preparation of freeze-dried precursors this solution was frozen instantly with liquid nitrogen and dried under vacuum (20–30 mbars) at −20 °C in an Alpha-Christ freeze-dryer. For the precursors obtained by the Pechini-type reaction, the La–Co–CA solution with La:Co:CA=1:1:10 was heated up to ~90 °C and ethylene glycol (EG) was added (CA:EG=1:4). The solution thus obtained was continuously stirred with a magnetic stirrer on a hot plate to remove the excess of water and to accomplish the polyesterification reaction. Prolonged heating produced a more and more viscous and bubbly pink mass. The thermal decomposition of the La–Co–Ni(Fe)-precursors was achieved at 400 °C for 3 h in air. The obtained solid residue was annealed between 600 and 900 °C for 20 h in air, then cooled down to room temperature at a rate of 5°/min. For the sake of convenience, the samples were further denoted as P-$LaCo_{1-x}M_xO_3$ and FD-$LaCo_{1-x}M_xO_3$ for oxides derived from Pechini-type precursors and from freeze-dried citrates, respectively.

The lanthanum, cobalt, nickel and iron content of the initial salt used was determined complexometrically. The mean oxidation state of the cobalt and nickel ions in the $LaCo_{1-x}Ni_xO_3$ samples was established iodometrically after dissolution of the powdered sample in HCl under argon. This method is not suitable for determination of the mean oxidation state of transition metal ions in $LaCo_{1-x}Fe_xO_3$ samples.

X-ray structural analysis was made on a Bruker Advance 8 diffractometer with Cu$K\alpha$ radiation. Step-scan recordings for structure refinement by the Rietveld method were carried out using 0.02° 2θ steps of 5 s duration.

Elastic coherent neutron scattering experiments were performed at the research reactor FRM-II (Garching n. Munich, Germany) on the high-resolution diffractometer SPODI [14]. Monochromatic neutrons ($\lambda=1.5482$ Å) were obtained at 155° take-off using the 551 reflection of a vertically-focused composite Ge monochromator. The vertical position-sensitive multidetector (300 mm effective height) consisting of 80 ^{3}He tubes and covering an angular spanning of 160° 2θ was used for data collection. Each sample (ca. 0.5 cm^3 in volume) was filled into a thin-wall (0.15 mm) vanadium can of 10 mm diameter. Two-dimensional powder diffraction data were collected at ambient temperature and then corrected for geometrical aberrations. The Rietveld refinement of X-ray and neutron diffraction data was carried out using the software package FullProf [15]. The peak profile shape was modeled by choosing pseudo-Voigt function. The scale factor, lattice parameter, fractional coordinate of atoms, their isotropic displacement parameters, zero angular shift, profile shape parameters and half width parameters were varied during the fitting. The background of the diffraction pattern was fitted using a linear interpolation between selected data points in non-overlapping regions.

The crystallite size of oxides was calculated by the Scherrer equation from the line width of the (012) and (024) reflection peaks: $D_{hkl}=\lambda/((\beta^2-\beta_o^2)^{1/2}\cos\theta_{hkl})$ where λ is Cu$K\alpha$ radiation, β is the peak width at the half height corrected with instrumental broadening and θ_{hkl} is the Bragg angle. The line width was determined by profile analysis using a WinPlotr program.

The thermal analysis (simultaneously obtained DTA, TG and DTG curves) of the precursors was performed by a "Stanton Redcroft" apparatus in the temperature range up to 650 °C in air, at a heating rate of 5 °C/min and sample mass of 10 mg.

The EPR spectra were recorded as the first derivative of the absorption signal of an ERS-220/Q spectrometer within the temperature range of 90–400 K. The g factors were determined with respect to a Mn^{2+}/ZnS standard. The signal intensity was established by double integration of the experimental EPR spectrum.

SEM images of powders coated with gold were obtained by a Zeiss DSM 962 microscope and by Philips XL30 scanning electron microscopes. TEM analysis was carried out with a Philips/FEI CM20 microscope, at an accelerating voltage of 200 kV. The specific surface area of the samples was determined by the BET method using low-temperature nitrogen adsorption.

Temperature programmed reduction (TPR) experiments were carried out in the measurement cell of a differential scanning calorimeter (DSC), model DSC-111 (SETARAM), directly connected to a gas chromatograph (GC), in the 300–973 K range at a 10 K/min heating rate in a flow of $Ar:H_2=9:1$, the total flow rate being 20 ml/min. A cooling trap between DSC and GC removes the water obtained during the reduction. To obtain the *ex-situ* XRD patterns of the partially reduced oxides, the reduction process was interrupted at selected temperatures and then the samples were cooled down to 250 °C with a rate of 40°/min and then to room temperature with a rate of 20°/min in an $Ar:H_2$ flow followed by Ar treatment for 10 min.

3. Results/discussions

3.1. Structure and morphology of $LaCo_{1-x}Ni_xO_3$ and $LaCo_{1-x}Fe_xO_3$

The organic component has been shown to be an important factor determining the thermal properties of the two types of the citrate precursors [13]. Fig. 1 gives the DTA, DTG and TG curves of freeze-dried citrates and Pechini-type precursors. For freeze-dried La–$Co_{0.9}Ni_{0.1}$ and La–$Co_{0.9}Fe_{0.1}$ citrates, the DTA curves display two endothermic processes at 145 and 170 °C, followed by exothermic processes at about 320 and 350 °C (Figs. 1A and B). According to the thermal properties of citrate complexes [16–20], the endothermic processes can be assigned to the dehydration and to the transformation of the citrate into aconitate, while the exothermic processes correspond to the combustion of the residual organics. For Pechini-type precursors, the decomposition starts at temperatures higher than that of freeze-dried citrates (above 250 °C, Figs. 1A and B). This is a consequence of the esterification reaction between the citric acid and the ethylene glycol, which proceeds together with complexation of the metal

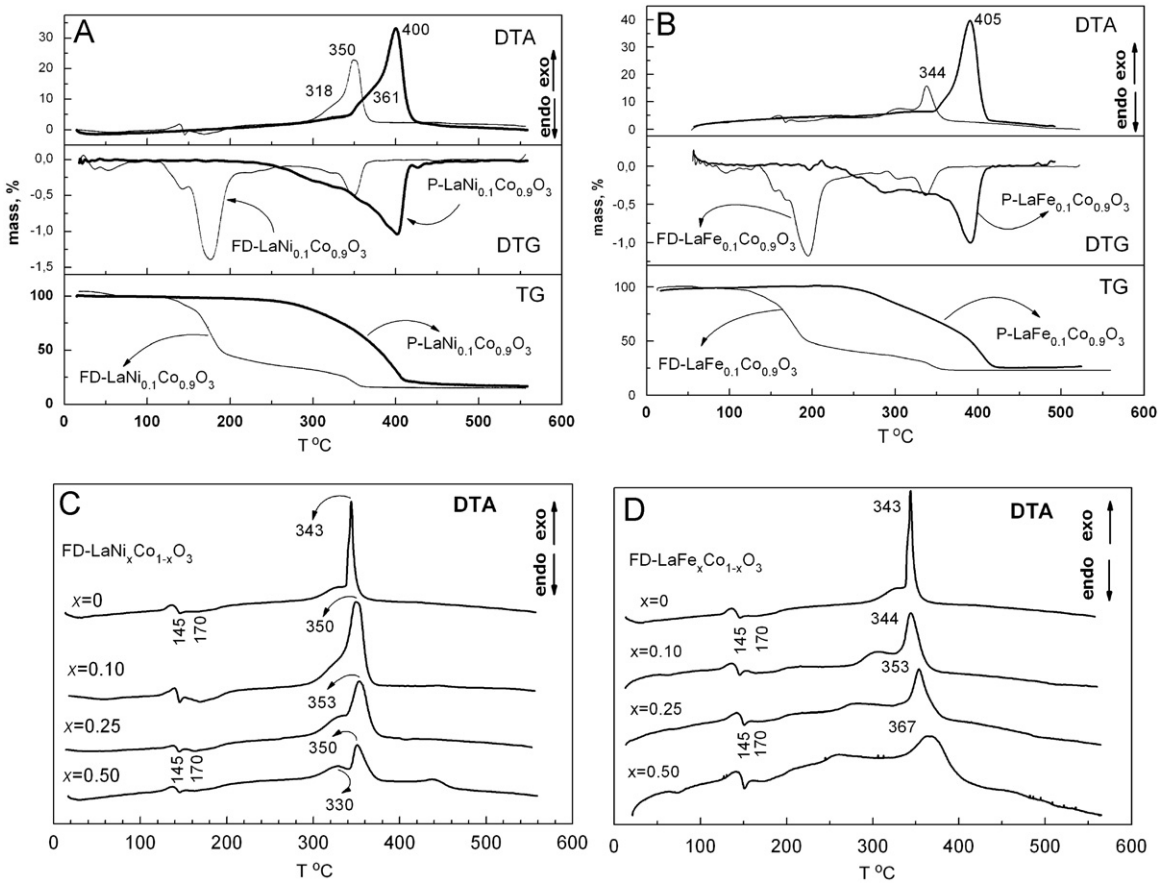

Fig. 1. DTA, DTG and TG curves of freeze-dried citrate precursors (thin lines) and Pechini-type precursors (thick lines) with La–$Co_{0.9}Ni_{0.1}$ (A) and La–$Co_{0.9}Fe_{0.1}$-compositions (B). DTA curves of freeze-dried La–$Co_{1-x}Ni_x$ (C) and La–$Co_{1-x}Fe_x$ (D) citrates are also given.

ions by citric acid [12,20]. Above 350 °C, there are exothermic peaks due to the vigorous combustion of the organics. The process is finished at 440 °C (a temperature higher than that of freeze-dried citrates, 360 °C). Above 440 °C, a slight weight loss (about 1%) is observed due to the burning of the deposited carbon. The same process of carbon burning is well established during thermal treatment of citrate complexes containing ethylene glycol [13,18,20].

Figs. 1C and D compare the DTA curves of freeze-dried La–$Co_{1-x}Ni_x$ and La–$Co_{1-x}Fe_x$ citrates with x varying from 0 to 0.5. By increasing the Ni and Fe content, the two endothermic peaks due to the dehydration and the transformation of the citrate into aconitate remain intact, whereas the exothermic peak due to the combustion of the residual organics is developed in a wider temperature range. It appears that the Ni and Fe amounts only slightly affect the decomposition process of the La–Co precursors.

At 400 °C for a short heating time (3 h), thermal decomposition of both freeze-dried and Pechini-type precursors yields a mixture of a perovskite phase ($LaCo_{1-x}Ni_xO_3$), spinel oxide ($Co_{3-y}Ni_yO_4$) and $La_2O_2CO_3$ (Fig. 2). This means that irrespective of the precursors used, the formation of the perovskite phase proceeds by the interaction of $La_2O_2CO_3$ with the spinel oxide. The same results are obtained for the iron-containing precursors. It is worth mentioning that unsubstituted $LaCoO_3$ display the same mechanism of formation from citrate precursors [13]. This is consistent with the thermal properties of both citrate precursors, where the organic component has a crucial role.

By increasing the preparation temperature from 400 to 600 °C and by prolonging the annealing time from 3 to 20 h, well-crystallized single phases of rhombohedrally distorted $LaCo_{1-x}Ni_xO_3$ and $LaCo_{1-x}Fe_xO_3$ perovskites were obtained by both methods (Fig. 3). Fig. 4 gives the lattice parameters as a function of the amount of Ni and Fe ions. The lattice parameter a that reflects the distance between two neighboring transition metal ions increases with the Ni and Fe content. A lattice expansion is also observed when $LaCo_{1-x}Ni_xO_3$ and $LaCo_{1-x}Fe_xO_3$ perovskites are annealed at 900 °C.

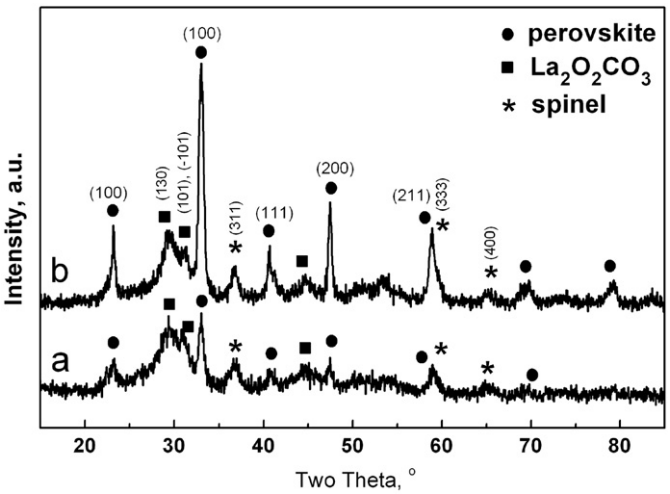

Fig. 2. XRD patterns of the thermal decomposition products of freeze-dried La–$Co_{0.9}Ni_{0.1}$-CA (a) and La–$Co_{0.9}Ni_{0.1}$-CA-EG precursors (b) at 400 °C. Bragg reflections for perovskite (●, $LaCo/NiO_3$), monoclinic $La_2O_2CO_3$ (■) and spinel phase (*) are given.

Irrespective of the annealing temperature, the Vegard's law is not obeyed. This is a consequence from the spin transitions of the Co^{3+} ions in cobalt perovskites. For pure $LaCoO_3$, the Co^{3+} ions are in a low-spin configuration ($S=0$) below 35 K; above 35 K, there is a transition from low-spin to high-spin Co^{3+} ($S=2$) culminating between 110 and 350 K in an ordered semiconducting phase containing about 50% high-spin and 50% low-spin ions [21,22]. When Ni is substituted for Co, the rhombohedrally distorted perovskite structure is preserved together with promotion of the high-spin state of the cobalt ions [23,24]. The ionic radii of high-spin Co^{3+} and Ni^{3+} are close (0.61 and 0.60 Å, respectively), whereas low-spin Ni^{3+} has a slightly larger ionic radius than that of low-spin Co^{3+} (0.56 and 0.545 Å, respectively) [25]. In addition, the lattice expansion can also be related with oxygen non-stoichiometry of $LaCo_{1-x}Ni_xO_3$. The mean oxidation state of the $Co_{1-x}Ni_x$ ions in $LaCo_{1-x}Ni_xO_3$ is shown in Fig. 5. With increasing Ni content, there is a deviation of the mean oxidation state from 3. Furthermore, the annealing temperature also affects the mean oxidation state. It is noticeable that the observed changes in the oxidation state proceed in the framework of the perovskite structure (Fig. 3). These results enable to relate the oxygen non-stoichiometry of $LaCo_{1-x}Ni_xO_3$ with the appearance of Ni^{2+}, in addition to the Co^{3+} and Ni^{3+} ions. The ionic radius of Ni^{2+} (0.69 Å, [25]) is larger than that of low- and high-spin Co^{3+} and Ni^{3+} ions, which leads to the lattice expansion of $LaCo_{1-x}Ni_xO_3$. In the case of Fe-substituted perovskites, the observed lattice expansion can be related with the larger ionic radius of high-spin Fe^{3+} ions: 0.645 Å [25]. The smooth increase in the lattice parameters indicates the formation of $LaCo_{1-x}Ni_xO_3$ and $LaCo_{1-x}Fe_xO_3$ solid solutions.

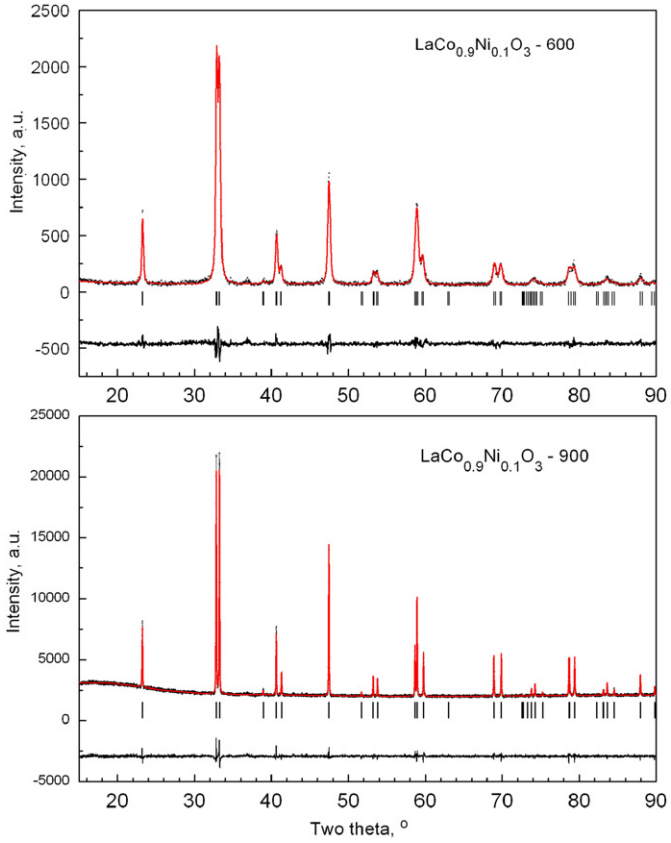

Fig. 3. XRD patterns of $LaCo_{0.9}Ni_{0.1}O_3$ obtained from freeze-dried citrates, annealed at 600 and 900 °C for 20 h.

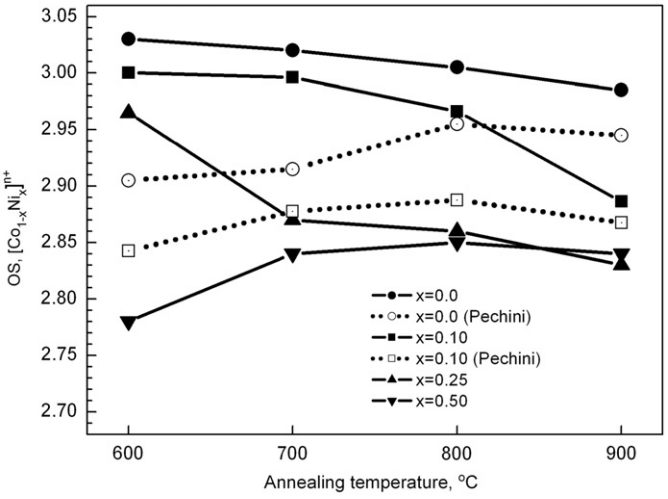

Fig. 5. Mean oxidation state of $[Co_{1-x}Ni_x]^{n+}$ ions in $LaCo_{1-x}Ni_xO_3$ obtained from freeze-dried citrates and by the Pechini method. The annealing temperature varies from 600 to 900 °C.

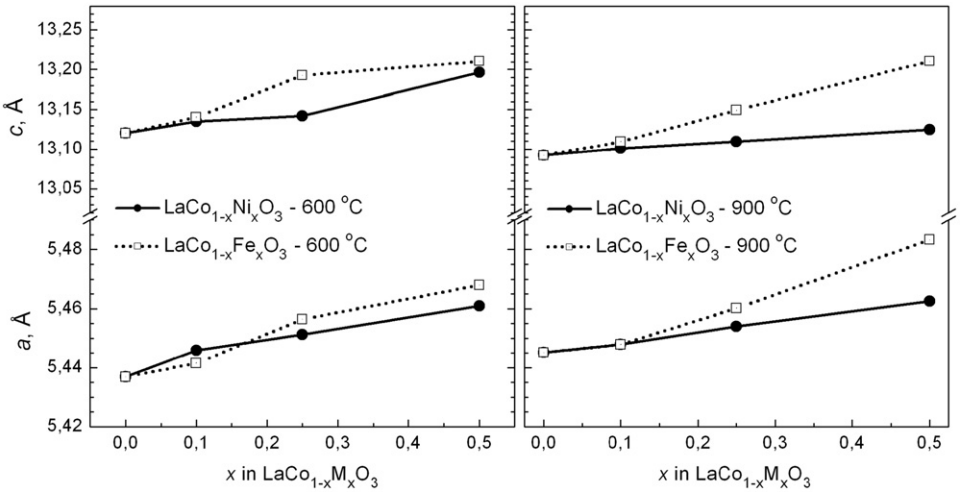

Fig. 4. Lattice parameters (a, c) for rhombohedrally distorted $LaCo_{1-x}Ni_xO_3$ and $LaCo_{1-x}Fe_xO_3$ obtained freeze-dried citrates, annealed at 600 and 900 °C.

The structural peculiarities of $LaCo_{1-x}Ni_xO_3$ and $LaCo_{1-x}Fe_xO_3$ solid solutions annealed at 900 °C were furthermore examined by means of neutron diffraction (Fig. 6). Analysis of neutron diffraction patterns shows that $LaCo_{1-x}Ni_xO_3$ and $LaCo_{1-x}Fe_xO_3$ adopt a rhombohedrally distorted perovskite structure, where Co and Ni/Fe ions are randomly distributed. Minor traces of impurities were detected by neutron diffraction experiments. Some reflections were attributed to La_2O_3 oxide, whereas other type of reflections does not fit to any known composition. Indexing of remaining reflections converged with a face-centered cubic lattice and lattice parameters ranging from ca. 8.35 to 8.57 Å, which is similar to spinel of Co_2CoO_4 type (Al_2MgO_4 type of structure). Numerous attempts to refine its crystal structure were unsuccessful, therefore this phase was included into the refinement via full profile decomposition (Le-Bail) technique. Furthermore the lattice parameter of the impurity spinel phase does not depend on the Ni/Fe-to-Co ratio and is higher than that of pure Co_3O_4: a=8.40–8.45 Å compared to a=8.08 Å, respectively. The appearance of the impurity phases is most probably a consequence of the perovskite formation by a solid state reaction of spinel oxides ($Co_{3-x}M_xO_4$) and $La_2O_2CO_3$. The same mechanism of perovskite formation from citrate-based precursors has recently been established for $(Ba_{0.5}Sr_{0.5})(Fe_{0.8}Zn_{0.2})O_{3-\delta}$ [26]. It has been demonstrated that the perovskite-type oxide is already formed at moderate temperatures (around 700 °C) via nano-scale solid state reactions between finely dispersed crystalline intermediates identified as a spinel and a carbonate [26].

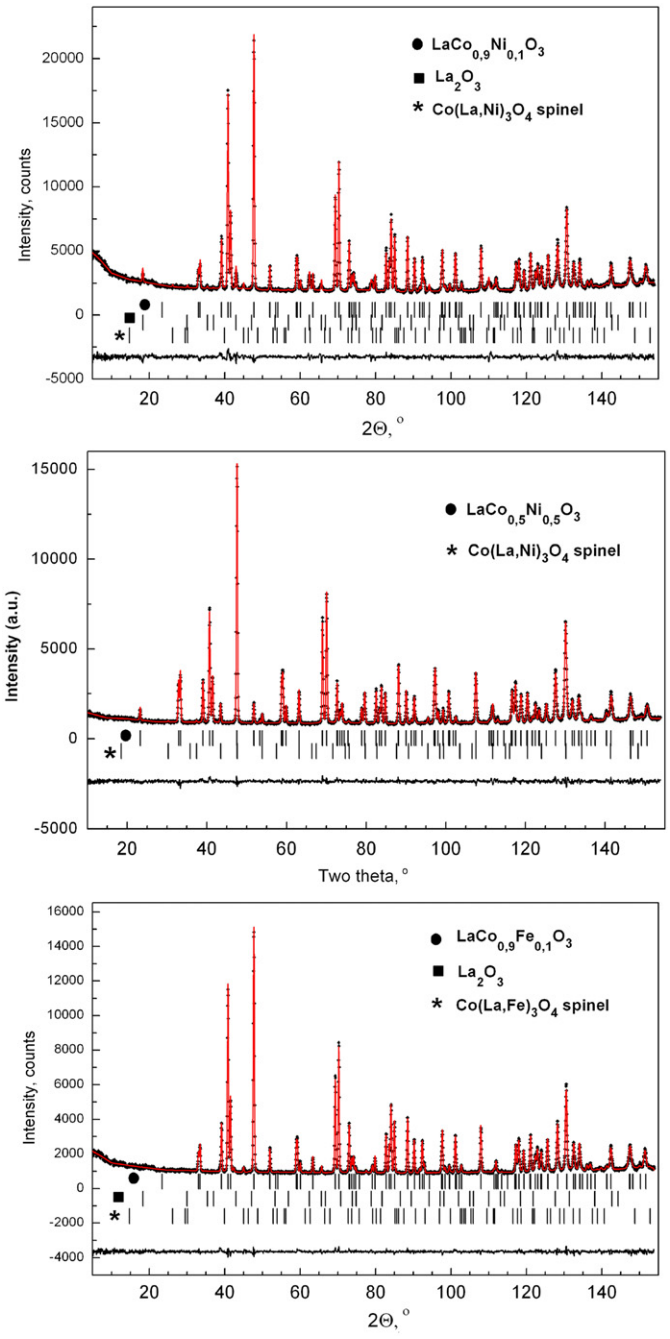

Fig. 6. Neutron diffraction patterns (points) of $LaCo_{0.9}Ni_{0.1}O_3$, $LaCo_{0.5}Ni_{0.5}O_3$ and $LaCo_{0.9}Fe_{0.1}O_3$ annealed at 900 °C. Calculated intensities (full lines) of Ni- and Fe-substituted perovskites at ambient temperature (λ=1.5482 Å). The difference curves are shown at the bottom. Bragg reflections for rhombohedrally distorted perovskite structure, impurities La_2O_3 and the spinel phases are indicated.

The obtained structural parameters are listed in Table 1. As it has been already seen with XRD the lattice expands upon Co to Ni/Fe substitution. An important feature is that the type of precursors used has no effect on the lattice parameters of Fe-substituted perovskites. On the contrary, Ni-substituted perovskites display slight changes in the lattice parameters when they are obtained from freeze-dried citrates or Pechini-type precursors. This is in agreement with the observed changes in the mean oxidation state of metal ions in $LaCo_{1-x}Ni_xO_3$ obtained by both methods (Fig. 5).

Free oxygen atomic coordinate x_O is not sensitive to the type of precursors and rather low isotropic displacement parameters B were found for all constituents thus indicating minor atomic disorder in the system.

The determination of occupancy factors in this system is a complicated procedure. In order to reduce the correlations between parameters, the oxygen occupation was given by the iodometric titration, whereas the total occupancy on 6a (La) and 6b sites (Co/Ni/Fe) was constrained to $\frac{1}{6}$ (Table 1). As one can see, this model describes well the cationic distribution in Ni and Fe-substituted perovskites.

The distribution of Ni and Fe in $LaCo_{1-x}Ni_xO_3$ and $LaCo_{1-x}Fe_xO_3$ solid solutions annealed at 600 °C was furthermore examined by means of electron paramagnetic resonance spectroscopy. This technique has been used to examine both the defect structure of $LaCoO_3$ and the cationic distribution in Ni-substituted $LaCoO_3$ [27–30]. For $LaCoO_3$, defects including ferromagnetic coupled Co^{3+} and Co^{4+} ions were detected by EPR [29]. The defect density was higher when $LaCoO_3$ was obtained from precursors containing a lower amount of the organic component [13]. When $LaCo_{1-x}Ni_xO_3$ oxides are annealed at a lower temperature (600 °C), the EPR spectra consist of a signal due to magnetic Ni clusters [30].

Here we are extending the EPR study to Ni and Fe substituted $LaCoO_3$ obtained from citrate and EG-citrate precursors. Fig. 7 shows the EPR spectra of $LaCo_{1-x}Ni_xO_3$ and $LaCo_{1-x}Fe_xO_3$ oxides annealed at 600 °C. It is worth mentioning that "defectless" $LaCoO_3$, $LaCo_{1-x}Ni_xO_3$ and $LaCo_{1-x}Ni_xO_3$ do not give an EPR response in the X-band experiments (9.2 GHz) [27–30]. However, the EPR spectra of Ni-substituted $LaCoO_3$ consist of a broad signal, which, according to our previous studies, is due to magnetic Ni clusters. The density of these clusters increases with the Ni content going through a maximum at x=0.25. Contrary to $LaCoO_3$ and Ni-substituted oxides, Fe-substituted oxides do not display any EPR signal in the temperature range of 100–400 K. On increasing the annealing temperature from 600 to 900 °C, all perovskites become EPR "silent".

The morphology of Ni- and Fe-substituted $LaCoO_3$ also depends on the synthesis procedure used (Fig. 8). At 600 °C, unsubstituted $LaCoO_3$ obtained from freeze-dried citrate displays

Table 1
Structural parameters of $LaCo_{1-x}Ni_xO_3$ and $LaCo_{1-x}Fe_xO_3$ at ambient temperature as obtained from treatment of neutron data by Rietveld method.

	FD-$LaNi_{0.10}Co_{0.90}O_3$	P-$LaNi_{0.10}Co_{0.90}O_3$	FD-$LaNi_{0.50}Co_{0.50}O_3$	P-$LaFe_{0.10}Co_{0.90}O_3$	FD-$LaFe_{0.10}Co_{0.90}O_3$
Phase 1 (perovskite)					
a (Å)	5.44502(8)	5.44728(8)	5.46068(8)	5.44418(7)	5.44424(8)
c (Å)	13.0930(2)	13.0960(2)	13.1190(2)	13.1025(2)	13.1016(2)
x_O, (rel. un.)	0.5499(1)	0.5500(1)	0.5504(1)	0.5498(1)	0.5500(1)
B_{La} (Å^2)	0.51(3)	0.52(4)	0.59(3)	0.41(3)	0.46
$B_{Co/Ni/Fe}$ (Å^2)	0.02(8)	0.23(9)	0.10(4)	0.41(7)	0.37(6)
B_O (Å^2)	0.67(2)	0.64(2)	0.58(2)	0.75(2)	0.71(2)
x_O	0.981	0.99(1)	0.974	1.0	1.0
$x_{Ni/Fe:Co}$	0.029(5):0.971(5)	0.065(6):0.935(6)	0.412(5):0.585(5)	0.115(6):0.885(6)	0.112(6):0.888(6)
IIR	92.82	97.42	94.83	97.05	96.09
R_{Bragg} (%)	2.80	2.35	2.68	2.49	2.74
Phase 2 (spinel)					
a (Å)	8.4469(3)	8.4371(5)	8.3575(3)	8.5651(8)	8.5600(7)
IIR	4.85	2.58	5.17	1.23	1.97
R_{Bragg} (%)	0.02	0.054	0.023	0.123	0.367
Phase 3 (La_2O_3)					
a (Å)	3.9434(4)			3.9426(6)	3.9421(6)
c (Å)	6.068(1)			6.064(1)	6.070(1)
IIR	2.33			1.72	1.94
R_{Bragg} (%)	0.08			0.451	0.572
R_p (%)	2.74	3.13	3.35	3.09	3.13
R_{wp} (%)	3.62	4.06	4.26	4.04	4.01
R_{exp} (%)	3.51	5.11	5.00	4.97	4.91

The space group is $R\bar{3}c$ (No. 167). The structural data were modeled for La occupying the 6*a* position (0,0,$\frac{1}{4}$), Co/Ni/Fe are located on 6*b* site (0,0,0), whilst oxygen occupy 18*e* position (x_O,0,$\frac{1}{4}$). Numbers in parentheses give statistical errors in the last significant digit. IIR denotes the mass fraction of phases.

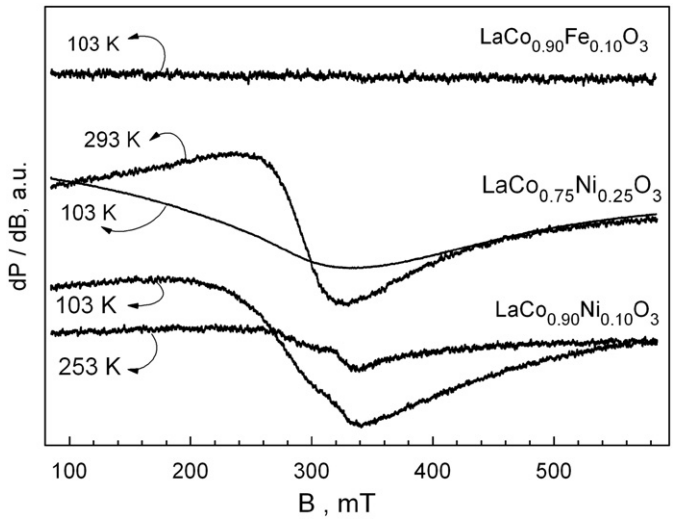

Fig. 7. EPR spectra of $LaCo_{0.9}Ni_{0.1}O_3$, $LaCo_{0.75}Ni_{0.25}O_3$ and $LaCo_{0.9}Fe_{0.1}O_3$ annealed at 600 °C.

plate-like aggregates with dimensions higher than 5 μm, whereas particles with lower extent of agglomeration are formed by the Pechini method. The presence of Ni and Fe reduces the extent of particle agglomeration.

Inside the aggregates, well-crystallized hexagonal individual particles become visible (Fig. 8g). The particle dimensions (about 70 ± 25 nm) fall in the nanometric scale and depend neither on the Ni and Fe content nor on the type of the precursor used. This insensitivity of the particle dimensions is further supported by the crystallite sizes determined from the broadening of (012) and (024) diffraction lines: 33 ± 4 and 41 ± 4 nm for $LaCo_{0.9}Ni_{0.1}O_3$ and $LaCo_{0.9}Fe_{0.1}O_3$, respectively. It is important that the particle dimensions determined by TEM analysis match the crystallite sizes determined from diffraction line broadening, indicating the formation of nanometric crystallites of perovskites.

With the increase of the annealing temperature, the aggregates disappear at the expense of the appearance of larger particles. At 800 °C, the powders obtained from freeze-dried citrates show a tendency to form an open network of well shaped particles, while the Pechini method yields submicron particles loosely connected by one another (Fig. 9). As in the case of perovskites annealed at low temperatures, the particle dimensions seem to be independent on the Ni and Fe ions: 400 ± 50 and 440 ± 50 nm for $LaCo_{0.9}Ni_{0.1}O_3$ and $LaCo_{0.9}Fe_{0.1}O_3$ annealed at 900 °C, respectively. They appeared to be slightly lower in comparison with that of unsubstituted $LaCoO_3$: 560 nm. It is worth mentioning that all samples display close particle size distribution.

The observed changes in the morphology are consistent with the specific surface area of the perovskites. For the perovskites annealed at 600 °C, the specific surface area varies between 12 and 15 m^2/g, while by increasing the annealing temperature up to 900 °C the specific surface area decreases to 1–2 m^2/g. Furthermore, the specific surface area is insensitive towards the Ni and Fe content, as well as towards the type of the precursor used.

3.2. Reducibility of $LaCo_{1-x}Ni_xO_3$ and $LaCo_{1-x}Fe_xO_3$

The structural and morphological characterizations enable to examine the reducibility of Ni and Fe substituted $LaCoO_3$. Fig. 10 compares the TPR curves of $LaCo_{1-x}Ni_xO_3$ and $LaCo_{1-x}Fe_xO_3$ annealed at 600 and 900 °C. In the TPR curves of Ni-substituted perovskites, two well separated peaks are distinguished: a low-temperature (LT) peak developed between 250 and 500 °C and a high-temperature (HT) peak appearing above 500 °C. Irrespective of the annealing temperature, the HT reduction peak is shifted towards lower temperature with increase in the Ni content. The same dependence on the Ni content is observed for the LT reduction peak, especially for perovskites annealed at 600 °C. Contrary to $LaCo_{1-x}Ni_xO_3$, the TPR curves of Fe-substituted perovskites display only the LT reduction peak, while the HT peak falls outside the temperature scale used. By increasing the Fe

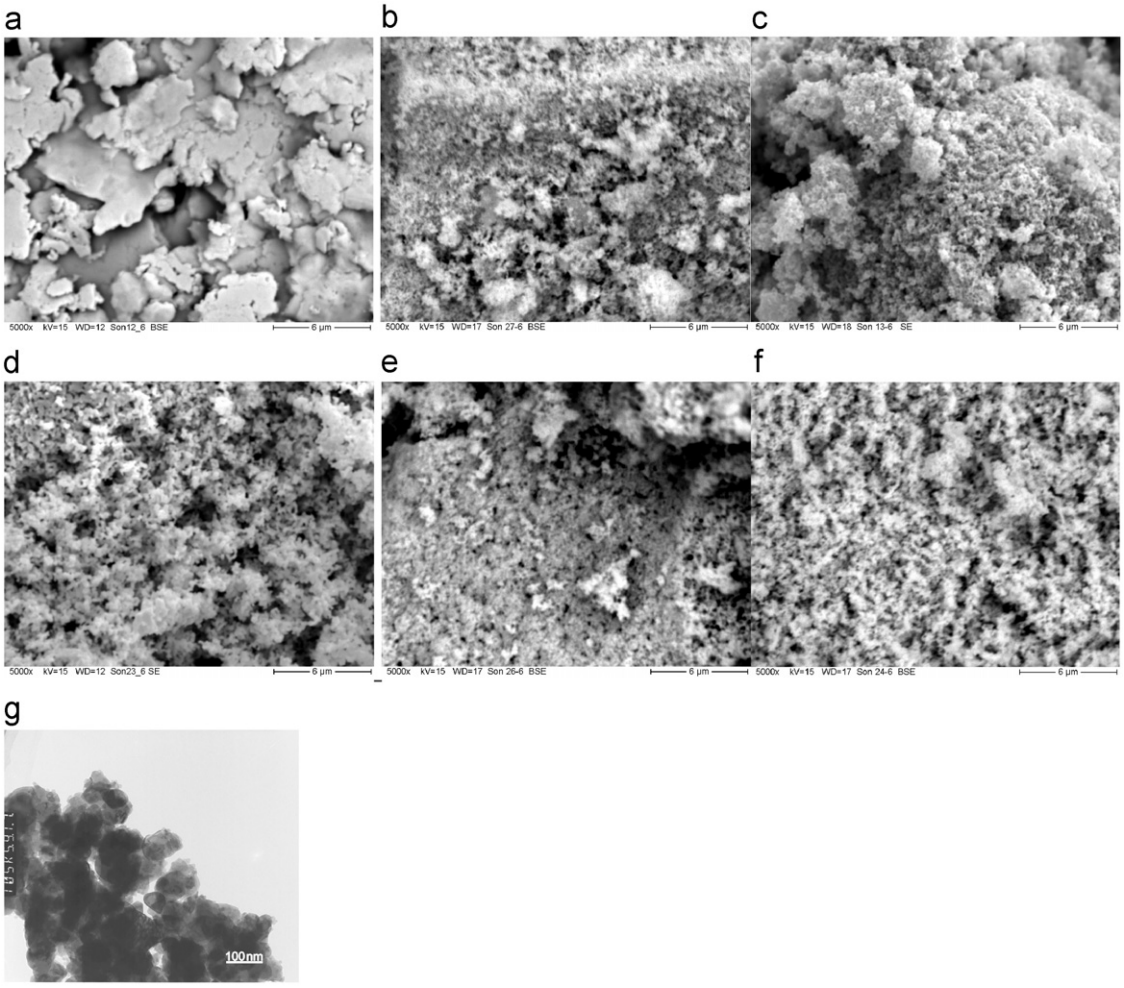

Fig. 8. SEM images of FD-$LaCoO_3$ (a), FD-$LaCo_{0.9}Ni_{0.1}O_3$ (b), FD-$LaCo_{0.9}Fe_{0.1}O_3$ (c), P-$LaCoO_3$ (d), P-$LaCo_{0.9}Ni_{0.1}O_3$ (e) and FD-$LaCo_{0.9}Fe_{0.1}O_3$ (f) annealed at 600 °C. TEM images of FD-$LaCo_{0.9}Ni_{0.1}O_3$ (g) annealed at 600 °C.

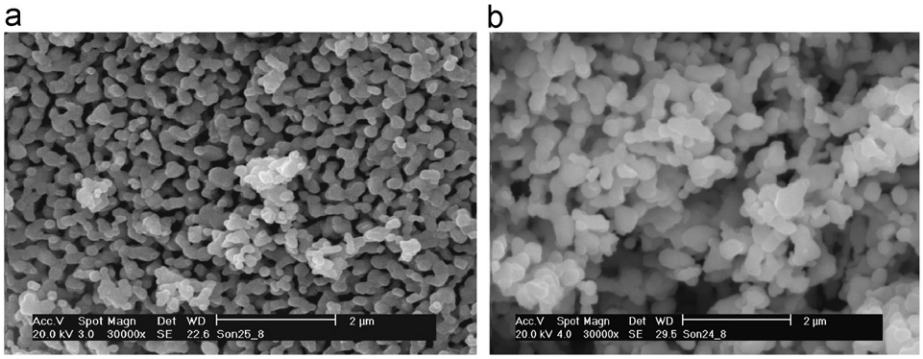

Fig. 9. SEM images of $LaCo_{0.5}Ni_{0.5}O_3$ obtained from freeze-dried citrates (a) and $LaCo_{0.9}Ni_{0.1}O_3$ obtained by the Pechini method (b). Annealing temperature is 800 °C.

content, the LT peak is progressively shifted towards higher temperatures, especially for the oxides annealed at 900 °C. From TPR analysis, two important features can be outlined. The first one indicates that the Fe-substituted perovskites are more stable in comparison with Ni-substituted ones. The second reveals that the reduction stability of the perovskites annealed at 600 °C is lower than that of perovskites annealed at 900 °C.

Furthermore, the reducibility of $LaCo_{1-x}Ni_xO_3$ and $LaCo_{1-x}Fe_xO_3$ perovskites displays a dependence on the type of the precursors used (Fig. 11). Perovskites obtained by the Pechini method are characterized by lower reduction stability as compared to the perovskites obtained from freeze-dried citrates. This dependence is well pronounced for $LaCoO_3$ and Ni-substituted $LaCoO_3$ only. The reducibility of Fe-substituted perovskites remains the same irrespective of the type of precursors used. It is worth mentioning that the specific surface area of the perovskites obtained from freeze-dried citrates and Pechini-type precursors is similar for one and the same annealing temperature.

To rationalize the reduction process of $LaCo_{1-x}Ni_xO_3$ and $LaCo_{1-x}Fe_xO_3$, *ex-situ* XRD measurements of partially and completely reduced perovskites were undertaken (Fig. 12). The reduced compositions were obtained after interruption of the

reduction process at selected temperatures corresponding to the LT and HT peaks (shown in the inset of Fig. 12). Irrespective of the Ni content and the annealing temperature, the complete reduction of $LaCo_{1-x}Ni_xO_3$ yields a mixture of La_2O_3 and transition metal (Fig. 12). The diffraction peak at about 44° due to metals is too broad, thus preventing one to specify if pure Co and Ni metals or $Co_{1-x}Ni_x$ alloys are formed.

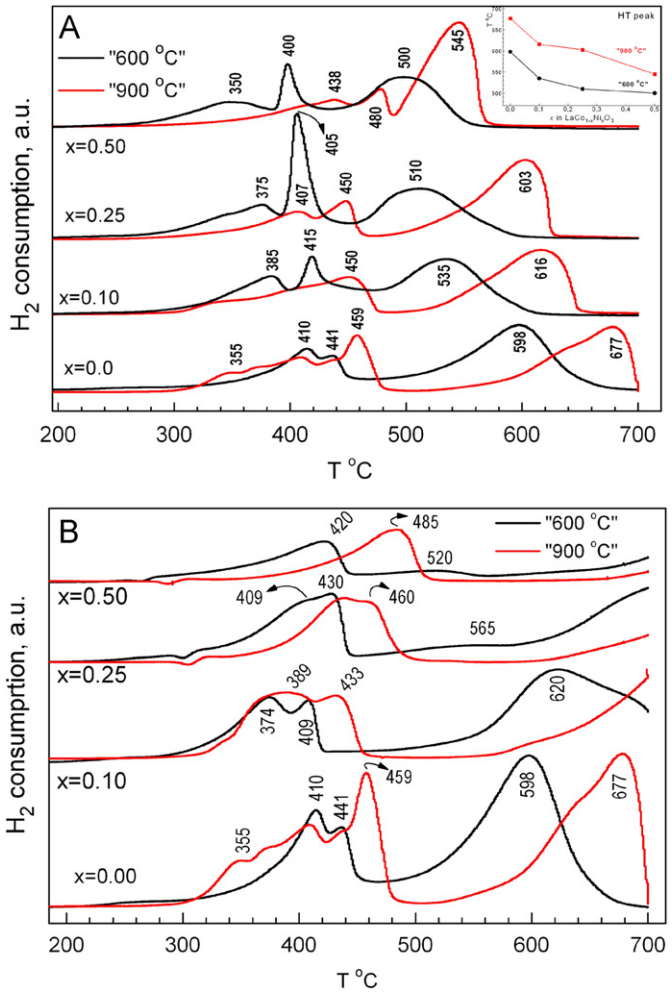

Fig. 10. TPR curves of $LaCo_{1-x}Ni_xO_3$ (A) and $LaCo_{1-x}Fe_xO_3$ (B) obtained from freeze-dried citrates, annealed at 600 and 900 °C. The inset shows the position of HT peak versus the Ni content for $LaCo_{1-x}Ni_xO_3$ (A).

The Ni content and the synthesis procedure affect the formation of intermediate products of perovskite reduction. After partial reduction up to 420 °C, oxygen-deficient perovskites are formed. By increasing the Ni content and the annealing temperature, the Brownmillerite type phase ($La_2Co_2O_5$) is stabilized. The unit cell parameters of the Browmnillerite phase deviate from that of unsubstituted $La_2Co_2O_5$: $a=5.4327$ Å, $b=15.8240$ Å, $c=5.6586$ Å for reduced $LaCo_{0.75}Ni_{0.25}O_3$ versus $a=5.4445$ Å, $b=15.8689$ Å, $c=5.6922$ Å for $La_2Co_2O_5$. This indicates that Ni ions are included into the $La_2Co_2O_5$ structure. In addition to the oxygen-deficient $LaCo_{1-x}Ni_xO_{3-y}$ phases, transition metals are also detected at the initial stage of reduction. The formation of transition metals proceeds more easily for the perovskites with the higher Ni content and when they are annealed at 600 °C. Rough estimation from the XRD patterns shows that for $LaCo_{0.75}Ni_{0.25}O_3$ annealed at 600 °C about 30% of the total amount of the transition metal is obtained during the reduction up to 420 °C whereas for the sample annealed at 900 °C this amount is about 20%.

In contrast to Ni substituted perovskites, the low-temperature reduction of Fe-substituted oxides (up to 450 °C) produces slight changes in the perovskite structure. The oxygen-deficient Brownmillerite type phase ($La_2Co_2O_5$) is stabilized only after the reduction of Fe-poor perovkites annealed at 900 °C. It is noticeable that, irrespective of the annealing temperature, the reduction of $LaCo_{1-x}Fe_xO_3$ takes place without the formation of Co and/or Fe metals.

Based on *ex-situ* XRD experiments, the reduction of Ni substituted perovskites can be described as a two-step process comprising the reduction of Co^{3+} and Ni^{3+} ions to Co^0 and Ni^0 metal via Co^{2+} and Ni^{2+} ions. At the first stage, there is a release of oxygen from the $LaCo_{1-x}Ni_xO_3$ perovskite leading to the formation of oxygen-deficient perovskite-related phases. Ni-poor perovskites annealed at 600 °C are capable to reversibly uptake oxygen, as a result of which the oxygen-deficient phase is not stable during the air exposure of the oxide for *ex-situ* XRD experiments. The reversible process of oxygen release and uptake is favored by the nanometric particle dimensions. By increasing the Ni content, oxygen-deficient perovskite-related phases from the Brownmillerite series, $La_n(Co_{1-x}Ni_x)_nO_{3n-1}$, become more stable. Above 500 °C, irreversible reduction of the oxygen-deficient perovskites to transition metals and lanthanum oxide takes place. The temperature of complete perovskite reduction smoothly decreases with increasing the Ni content. Contrary to $LaCo_{1-x}Ni_xO_3$, Fe-substituted perovskites display higher reduction stability, as a result of which, only the first stage of the reduction process is accomplished between 200 and 700 °C. By increasing the Fe content, oxygen-deficient perovskites,

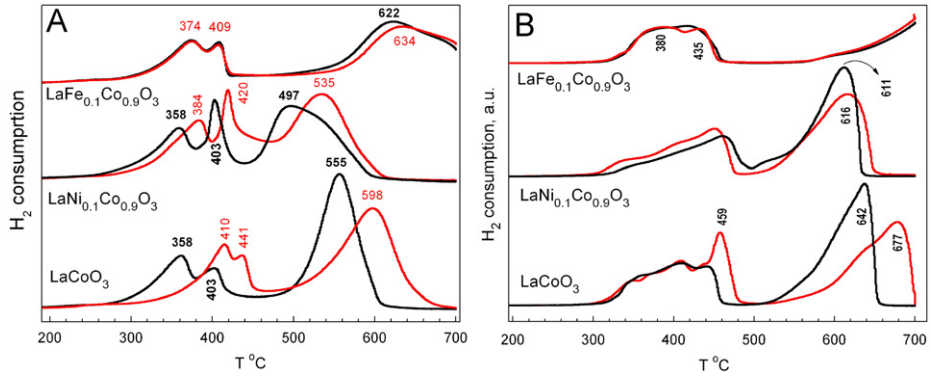

Fig. 11. TPR curves of $LaCoO_3$, $LaCo_{0.9}Ni_{0.1}O_3$ and $LaCo_{0.9}Fe_{0.1}O_3$ annealed at 600 °C (A) and 900 °C (B), obtained from freeze-dried citrates (red curves) and by the Pechini method (black curves). (For interpretation of the references to color in this figure legend, the reader is referred to the web version of this article.)

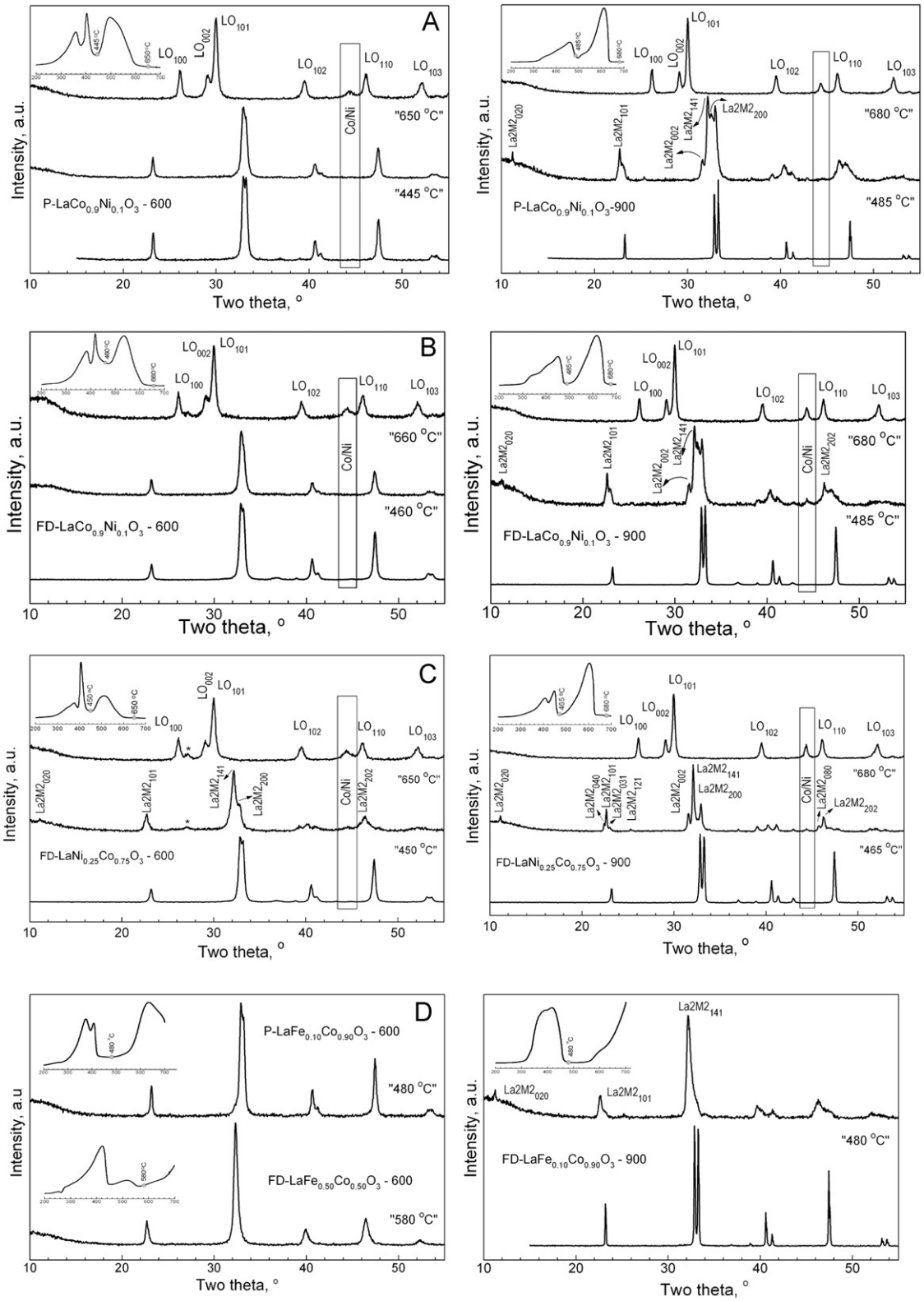

Fig. 12. XRD patterns of partially reduced oxides derived from P-$LaCo_{0.9}Ni_{0.1}O_3$ (A), FD- $LaCo_{0.9}Ni_{0.1}O_3$ (B), FD-$LaCo_{0.75}Ni_{0.25}O_3$ (C) and FD-$LaCo_{1-x}Fe_xO_3$ with $x=0.1$ and $x=0.5$ (D). The annealing temperature (marked in the figure) is 600 °C (left) and 900 °C (right). The inset shows the temperature where the reduction process is interrupted. Bragg reflections for $La_2M_2O_5$ ($La_2M_{2\,hkl}$), La_2O_3 (LO_{hkl}) and Co/Ni metal (Co/Ni_{hkl}) are given.

$LaCo_{1-x}Fe_xO_{3-x}$, become more stable than the Brownmillerite-phase, $La_n(Co_{1-x}Fe_x)_nO_3$.

Depending on the synthesis procedure, Ni-substituted perovskites display a deviation from the two-step reduction reaction with formation of transition metals between 250 and 500 °C (i.e. the temperature range where the LT peak is developed). To outline this peculiarity, the ratio of the HT to LT peak area is determined. The peak areas were estimated by

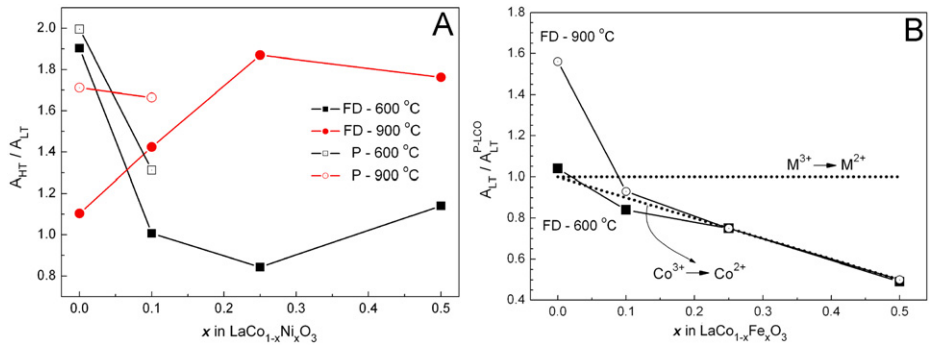

Fig. 13. The HT-to-LT area ratio (A_{HT}/A_{LT}) for FD-$LaCo_{1-x}Ni_xO_3$ and P-$LaCo_{1-x}Ni_xO_3$ annealed at 600 and 900 °C (A). The normalized LT peak area of $LaCo_{1-x}Fe_xO_3$ annealed at 600 and 900 °C (B). The calculated ones for two-step reduction mechanism and for preferential reduction of Co^{3+} to Co^{2+} are shown with dotted lines.

numerical integration of the curves between 250 and 480 °C and between 480 and 700 °C for the LT and HT peaks, respectively. Fig. 13A gives the HT-to-LT area ratio as a function of the Ni-content. When the perovskite reduction proceeds by consecutive formation of M^{2+} and metal phases, the ratio of the areas of the HT-to-LT peaks has to be equal to 2. This value will be slightly higher than 2, if we take into account the oxygen non-stoichiometry of $LaCo_{1-x}Ni_xO_3$ (Fig. 5). The formation of a transition metal during the first stage of reduction will diminish the ratio of the areas of the HT-to-LT peaks. As one can see, for Ni-rich perovskites annealed at 900 °C the deviation from the two-step reduction process is less obvious. The reduction reaction is more complex for Ni-poor perovskites and for perovskites annealed at 600 °C and includes the formation of both oxygen-deficient perovskites and transition metal. In addition, the reduction process is sensitive towards the type of precursors used. Perovskites obtained from Pechini-based precursors are reduced in two steps, while a deviation from two-step reduction reaction is observed for perovskites obtained from freeze-dried citrates.

The effect of the synthesis procedure on the reducibility of $LaCo_{1-x}Ni_xO_3$ can be related to their stoichiometry and morphology. The more non-stoichiometric is $LaCo_{1-x}Ni_xO_3$, the more easily the Brownmillerite-type perovskite is stabilized as an intermediate product of $LaCo_{1-x}Ni_xO_3$ reduction. The loosely bonded nanometric particles make the one-step reduction of M^{3+} to M^0 easier. The appearance of spinel impurities, characterized with lower reduction stability than that of perovskites [31], can also contribute to the formation of transition metal at the first stage of the perovskite reduction. Taking into account the small amount of the spinel phase (less than 5%), it seems that most of the transition metal is formed after perovskite reduction.

In order to analyze the reduction behavior of Fe-substituted perovskites, $LaCoO_3$ obtained by the Pechini method is used as standard for Co^{3+}–Co^{2+} reduction between 250 and 500 °C. Fig. 13B gives the area of the LT peak of $LaCo_{1-x}Fe_xO_3$ normalized versus the area of the LT peak of P-$LaCoO_3$. As one can see, the normalized LT peak area decreases with the Fe content. To explain this observation, the same figure also presents the calculated normalized LT peak area supposing that Co^{3+} is reduced to Co^{2+} prior to Fe^{3+} ions. The comparison shows that there is a good agreement between experimentally determined and calculated ones. The preferential reduction of Co^{3+} to Co^{2+} is also consistent with XRD patterns of Fe-rich compositions reduced to 480 °C (Fig. 12).

The effect of Ni and Fe on the reduction stability of $LaCoO_3$ is consistent with data reported in the literature [32,33]. The two-step reduction via formation of Brownmillerite type phases has also been reported for the $LaCoO_3$ and $LaNiO_3$ compositions [34–42]. In addition, for $LaCoO_3$ and $LaNiO_3$, another reduction mechanism has been proposed: the interaction of perovskites with H_2 has been explained by the formation of Ruddlesden-Popper phases instead of Brownmillerite-type oxides [43,44]. In this case, a formation of transition metal together with Ruddlesden-Popper phases has been established [45]. The reduction of $LaFeO_3$ with H_2 is limited in the temperature range of 200–700 °C and proceeds via reduction of a small fraction of Fe^{4+} to Fe^{3+} ions [46,47]. In this study, we demonstrate that the reduction of Ni and Fe-substituted $LaCoO_3$ perovskites proceeds in two steps via the formation of oxygen-deficient perovskites. Depending on the synthesis procedure, the *ex-situ* XRD experiments show the formation of transition metal in addition to the oxygen-deficient perovskites. It is noticeable that, contrary to pure $LaCoO_3$ [13], no Ruddlesden-Popper phases are detected for Ni- and Fe-substituted perovskites.

4. Conclusions

The formation of $LaCo_{1-x}Ni_xO_3$ and $LaCo_{1-x}Fe_xO_3$ starts at 400 °C by the reaction between $La_2O_2CO_3$ and a spinel phase after the decomposition of the organic components. The solid state reaction proceeds at a nano-scale level, as a result of which well-crystallized $LaCo_{1-x}Ni_xO_3$ and $LaCo_{1-x}Fe_xO_3$ with a rhombohedrally distorted perovskite type structure are formed at 600 °C. These oxides display oxygen deficit when they are obtained via the Pechini route. For $LaCo_{1-x}Ni_xO_3$, the Co/Ni distribution is not completely homogeneous due to the formation of Ni magnetic clusters. On increasing the annealing temperature from 600 to 900 °C, a homogeneous Ni and Co distribution is observed. In the same sequence, the oxygen non-stoichiometry increases. For $LaCo_{1-x}Fe_xO_3$, a homogeneous Co and Fe distribution is achieved irrespective of the annealing temperature.

The morphology of $LaCoO_3$ obtained from freeze-dried citrates and annealed at 600 °C consists of plate-like aggregates with dimensions larger than 5 μm, whereas particles with lower extent of agglomeration are formed by the Pechini method. The presence of Ni and Fe reduces the extent of particle agglomeration. Inside the aggregates, well-crystallized nanoparticles with dimensions insensitive towards the Ni and Fe contents (70 ± 25 nm) are formed. With the increase in annealing temperature, crystallite growth takes place, the close particle distribution being preserved.

The complete reduction of $LaCo_{1-x}Ni_xO_3$ with H_2 proceeds to transition metal and La_2O_3. Both the Ni content and the synthesis procedure affect the formation of intermediate products of perovskite reduction. For Ni-rich perovskites ($x > 0.1$) annealed at 900 °C, the reduction proceeds via the formation of Brownmillerite type phases (Ni substituted $La_nCo_nO_{3n-1}$), while, for low-temperature annealed perovskites, the reduction reaction is more complex

including the formation of both oxygen-deficient perovskites and transition metal. The more non-stoichiometric $LaCo_{1-x}Ni_xO_3$ in respect of oxygen, the easier the Brownmillerite-type perovskite is stabilized as an intermediate product. The loosely bonded nanometric particles and the inhomogeneous distribution of Ni and Co ions favor the one-step reduction of M^{3+} to M^0.

The interaction of $LaCo_{1-x}Fe_xO_3$ with H_2 is not complete up to 700 °C. The reaction proceeds by preferential oxidation of Co^{3+} to Co^{2+} without affecting the Fe^{3+} ions.

The reduction of $LaCo_{1-x}Ni_xO_3$ and $LaCo_{1-x}Fe_xO_3$ is less sensitive towards the synthesis procedure as compared to unsubstituted $LaCoO_3$.

Acknowledgments

S.I. is grateful to EC for a grant within the FAME project (FAME FP6-500159-1). The authors are grateful to the financial support from the National Science Fund of Bulgaria (IDEAS no. D0-02-309/2008). E.Zh, R.S. and S.I. acknowledge the partial financial support by the National Science Fund of Bulgaria (National Centre for New Materials UNION, Contract no. DO-02-82/2008).

References

[1] M.A. Peña, J.L.G. Fierro, Chem. Rev. 101 (2001) 1981–2017.
[2] N.P. Brandon, S. Skinner, B.C.H. Steele, Ann. Rev. Mater. Res. 33 (2003) 183–213.
[3] F. de Bruijn, Green Chem. 7 (2005) 132–150.
[4] H. Tanaka, M. Misono, Current Opinion in Solid State Mater. Sci. 5 (2001) 381–387.
[5] A. Mai, F. Tietz, D. Stöver, Solid State Ionics 173 (2004) 35.
[6] F. Tietz, A. Mai, D. Stöver, Solid State Ionics 179 (2008) 1509.
[7] A. Boreave, H. Tan, V. Roche, Ph. Vernoux, J.P. Deloume, Solid State Ionics 179 (2008) 1071.
[8] S. Stølen, E. Bakken, C.E. Mohn, Phys. Chem. Chem. Phys. 8 (2006) 429–447.
[9] M.P. Pechini, US Patent No 3,330,697, 1967.
[10] M. Popa, M. Kakihana, Solid State Ionics 151 (2002) 251.
[11] A. Worayingyong, P. Kangvansura, S. Ausadasuk, P. Praserthdam, Colloids Surf. A 315 (2008) 217.
[12] A. Gaki, O. Anagnostaki, D. Kioupis, T. Perraki, D. Gakis, G. Kakali, J. Alloys Compd. 451 (2008) 305.
[13] S. Ivanova, A. Senyshyn, E. Zhecheva, K. Tenchev, V. Nikolov, R. Stoyanova, H. Fuess, J. Alloys Compd. 480 (2009) 279.
[14] M. Hoelzel, A. Senyshyn, R. Gilles, H. Boysen, H. Fuess, Neutron News 18 (2007) 23.
[15] J. Rodríguez-Carvajal, in: Satellite Meeting on Powder Diffraction of the XV Congress of the IUCr, 1990, p. 127.
[16] D. Hennings, W. Mayr, J. Solid State Chem. 26 (1978) 329.
[17] R. Robert, L. Bocher, B. Sipos, M. Döbeli, A. Weidenkaff, Prog. Solid State Chem. 35 (2007) 447.
[18] E. Zhecheva, R. Stoyanova, M. Gorova, R. Alcantara, J. Morales, J.-L. Tirado, Chem. Mater. 8 (1996) 1429.
[19] R. Alcantara, P. Lavela, J.-L. Tirado, R. Stoyanova, E. Kuzmanova, E. Zhecheva, Chem. Mater. 9 (1997) 2145.
[20] N. Petrova, D. Todorovsky, Mater. Res. Bull. 41 (2006) 576.
[21] M.A. Senaris-Rodrigues, J.B. Goodenough, J. Solid State Chem. 116 (1995) 224.
[22] M.A. Senaris-Rodrigues, J.B. Goodenough, J. Solid State Chem. 118 (1995) 323.
[23] J. Pérez, J. García, J. Blasco, J. Stankiewicz, Phys. Rev. Lett. 80 (1998) 2401.
[24] M.T. Escote, C.H. Westphal, R.F. Jardim, J. Appl. Phys. 87 (2000) 5908.
[25] R.D. Shannon, Acta Crystallogr. Sect. A 32 (1976) 751.
[26] A. Feldhoff, M. Arnold, J. Martynczuk, Th.M. Gesing, H. Wang, J. Solid State Chem. 10 (2008) 689.
[27] L. Armelao, G. Bandoli, D. Barreca, M. Bettinelli, G. Bottaro, A. Caneschi, Surf. Interface Anal. 34 (2002) 112.
[28] C. Oliva, S. Cappelli, A. Kryukov, G.L. Chiarello, A.V. Vishniakov, L. Forni, J. Mol. Catal. A Chemical 247 (2006) 248.
[29] S. Ivanova, E. Zhecheva, R. Stoyanova, J. Phys. Chem. Solids 68 (2007) 168.
[30] S. Ivanova, E. Zhecheva, R. Stoyanova, Phys. Stat. Sol. A 205 (2008) 1685.
[31] D. Shanke, S. Vada, E.A. Hilmen, A. Hoff, J. Catal. 156 (1995) 85.
[32] G. Sierra Gallego, C. Batiot-Dupeyrat, J. Barrault, E. Florez, F. Mondragón, Appl. Catal. A 334 (2008) 251.
[33] G. Valderrama, A. Kiennemann, M.R. Goldwasser, Catal. Today 133–135 (2008) 142.
[34] T. Nakamura, G. Petzov, L.J. Gauckler, Mater. Res. Bull. 14 (1979) 649.
[35] M. Crespin, W.K. Hall, J. Catal. 69 (1981) 359.
[36] M. Radovic, S.A. Speakman, L.F. Allard, E.A. Payzant, E. Lara-Curzio, W.M. Kriven, J. Lloyd, L. Fegely, N. Orlovskaya, J. Power Sources 184 (2008) 77.
[37] W.P. Finlandés, Solid State Ionics 129 (2000) 145.
[38] F. Martínez, C. Batiot-Dupeyrat, G. Valderrama, J. Tatibouët, Comptes Rendus Acad. Sci. Paris Serie IIc Chimie 4 (2001) 49.
[39] O.H. Hansteen, H. Fjellvåg, B.C. Hauback, J. Mater. Chem. 8 (1998) 2081.
[40] K. Vidyasagar, A. Reller, J. Gopalakrishnan, C.N.R. Rao, J. Chem. Soc. Chem. Commun. (1985) 7.
[41] B. Gilbu Tilset, H. Fjellvåg, A. Kjekshus, J. Solid State Chem. 119 (1995) 271.
[42] G.L. Charello, J.-D. Grunwald, D. Ferri, F. Krumeich, C. Oliva, L. Forni, A. Baiker, J. Catal. 252 (2007) 127.
[43] L. Huang, M. Bassir, S. Kaliaguine, Appl. Surf. Sci. 243 (2005) 360.
[44] E.A. Lombardo, K. Tanaka, I. Toyoshima, J. Catal. 80 (1983) 340.
[45] C. Batiot-Dupeyrat, G. Valderrama, A. Meneses, F. Martinez, J. Barrault, J.M. Tatibouët, Appl. Catal. A Gen. 248 (2003) 143.
[46] P. Ciambelli, S. Cimino, G. Lasorella, L. Lisi, S. De Rossi, M. Faticanti, G. Minelli, P. Porta, Appl. Catal. B 37 (2002) 23.
[47] P. Ciambelli, S. Cimino, S. De Rossi, L. Lisi, G. Minelli, I. Pettiti, P. Porta, G. Russo, Appl. Catal. B 29 (2001) 239.